THERMITE-FOR-DEMISE (T4D): MANUFACTURING AND CHARACTERIZATION OF SINTERED THERMITE PELLETS

Jacopo DOMASCHIO,[1] *Carlo ZANARDI,*[1] *Antonio M. GRANDE,*[1] *Alessandro FINAZZI,*[1] *Stefania CARLOTTI,*[1] *Christian PARAVAN,*[1] *and Filippo MAGGI*[1]

[1]*Dept. of Aerospace Science and Technology, Politecnico di Milano, Milan, Italy*

filippo.maggi@polimi.it · www.polimi.it

Abstract

The EIC THREAD project is currently examining the potential of shape-retentive thermite charges to support spacecraft disintegration during atmospheric re-entry. Pellets of Al/WO_3 with different oxidizer-to-fuel ratio were produced by pressing and sintering in high-vacuum at 600°C. Microscopy revealed that matching particle sizes between the Al matrix and the oxide is crucial for effective diffusion bonding. Sintered pellets showed expansion, likely due to WO_3 crystal phase transition at 550°C. Compaction levels between 75–90% of TMD were achieved, depending on oxide content. Mechanical strength improved significantly post-sintering. However, brittleness increased with higher oxide mass fraction, particularly above 40%. Ignition temperatures in air averaged ~1200°C across compositions, with sintered pellets consistently igniting, unlike loose powders. This suggests sintering reduces diffusion barriers, enhancing reaction propagation. Two combustion modes were observed: a violent "demising" behavior causing complete destruction of the pellet and heating element, and a milder "non-demising" mode. These are believed to be influenced by oxide distribution and O/F ratio.

KEYWORDS: thermite, sintering, tungsten trioxide, combustion, uniaxial compression.

1. Background

The accumulation of non-functional, human-made objects in Earth orbit—known as space debris—has accelerated in recent years [1, 2], posing a serious threat to the sustainability of space operations. Debris increases collision risk for active satellites, potentially triggering a cascade effect known as the Kessler syndrome [3]. Low Earth Orbit (LEO) is currently the most congested region. Regulations now require spacecraft to be removed from LEO within five years of mission end [4, 5], typically through atmospheric re-entry. This demands reliable disposal strategies that ensure complete disintegration and minimal ground risk.

Controlled re-entry, which directs the spacecraft to a remote area via a dedicated maneuver, is one option. However, it requires additional propellant and introduces a further point of failure [6]. These limitations highlight the need for passive approaches that enable safe, uncontrolled re-entry.

Design-for-Demise (D4D) involves designing spacecraft to fully disintegrate during re-entry, thereby reducing casualty risk without relying on controlled maneuvers [7]. ESA promotes D4D as the preferred solution for LEO missions [5]. Existing D4D methods vary widely in physical principles and Technology Readiness Level (TRL) [7].

Thermite-for-Demise (T4D) is a novel D4D approach that uses thermite reactions to aid spacecraft destruction during re-entry [8]. Thermites are highly energetic mixtures of metals and metal oxides that release heat as they undergo a redox reaction. Known for their high flame temperatures, low sensitivity, and tunability, they are used in rail welding, underwater metal cutting, and pyrotechnics [9, 10, 11, 12]. In T4D, thermite charges are embedded within spacecraft components to enhance ablation, breach structural elements, and induce controlled fragmentation [13, 14]. While wind tunnel tests have confirmed the concept [8, 15, 16, 17], the technology remains at a low TRL (<3–4).

Previous tests used thermite in powder or pellet form, which lack structural integrity and require containment. This leads to several issues: risk of contaminating nearby systems, inefficient heat transfer, unreacted material loss, and pressure buildup inside the thermite vessel, potentially leading to its fragmentation. These limitations call for an improved T4D concept.

Structural Reactive Materials (SRMs) offer a potential solution, combining energetic performance with mechanical strength. Hastings and Dreizin provide a comprehensive overview of the subject [18]. It has been demonstrated that thermite can be shaped into defined geometries via 3D printing of thermite-filled pastes [19]. The technique resembles additive manufacturing of cementitious materials [20]. The printed parts retain reactivity and deliver heat without needing external fixtures. However, the binders used so far seem poorly suited for space use. The development of thermite-based SRMs capable of shape retention and load-bearing throughout a spacecraft's lifetime remains an open research area, which is currently being explored within the European Innovation Council (EIC) THREAD project.

2. Sintering technology applicability to thermites

This work presents recent advancements in the shaping and characterization of thermite charges produced using the classic Powder Metallurgy (PM) press-and-sinter method. The concept exploits the similarities of thermites with Metal Matrix Composites (MMCs)[21]. MMCs are produced starting from powders via metal-additive sintering. The inclusion of additives allows for the tuning of certain effective properties of the final product, like stiffness, wear resistance, and thermal expansion coefficient. During the sintering process, the additive powder can be considered inert. The metal particles, on the other hand, undergo sintering and form the matrix which provides structural integrity. In this context, a thermite can be seen as a composite metal material, where the matrix is the metal fuel (*e.g.*, aluminum powder), and the additive is the metal oxide (*e.g.*, hematite).

One of the main challenges of this concept lies in the proper selection of the powders. The proportion of the components influences the thermite's stoichiometry by adjusting the oxidizer-to-fuel (O/F) ratio, and also impacts the sintering process by introducing non-bonding particles that hinder consolidation. A volume fraction of additives of roughly 30% has been identified as the upper threshold for maintaining effective sintering performance [21]. The particle size distribution of the powders plays a crucial role in determining the reactivity of the initial mixture [22], which must be carefully controlled to prevent premature thermite ignition during sintering. This distribution is equally important for the metal matrix, as it affects the initial packing density and the mechanisms of densification, thereby influencing overall sintering efficiency [21]. In practice, matching the particle size of the matrix and additive is often preferred, as it promotes more homogeneous dispersion of the additive within the matrix [23].

Exploratory manufacturing and mechanical tests were conducted by the authors on the common thermite blend of aluminum and iron oxide [24]. Lab-scale procedures and parameters for pressing and sintering were developed starting from a comprehensive literature survey. The process was proved effective by successful sintering of pure aluminum powder pellets, which showed very high compaction ($\geq$ 90% TMD), a yield stress of 30 MPa, in accordance with typical values reported for the virgin material [25], and a distinct ductile response to uniaxial compression. Sintered thermite pellets exhibited poor mechanical performance and brittle behavior even at low iron oxide mass fraction. The cause of this phenomenon was attributed to the relatively low size of the iron oxide particles, which impeded diffusion bonding in the coarser Al powder. Optical and Scanning Electron Microscope (SEM) images reinforced that hypothesis. In the present work, the selection of a different metal oxide which is more suitable for the production of a sintered thermite piece is discussed.

3. Materials and methods

3.1 Powder selection

A total of 30 Al-based, thermite formulations were considered. Aluminum was selected for the fuel matrix because *i*) the previously developed sintering process was successful with pure Al, and *ii*) Al is a good reducing agent for high temperature thermites. Spherical, micrometric Al was chosen to exploit its advantages with respect to nanometric Al: reduced handling risks (lower reactivity and volatility), higher metallic content, and lower cost [26].

The selection of the oxide was carried out according to the following logic. First, the formulations were ranked in descending order of Al volumetric fraction under the hypothesis of perfect packing (no voids) and stoichiometric composition. The assumption behind this criterion is that a high Al volumetric fraction is desirable for sintering, based on previous experience and literature [21]. The resulting formulations were then sifted based on the following criteria:

- Reactants shall be non toxic and non radioactive to reduce handling risks, and shall not contain rare-earth metals
- Limited gas phase products ($\leq$ 15%); the threshold is set at twice the expected gas production of the legacy aluminum/iron oxide thermite
- High adiabatic flame temperature ($\geq$ 2500 K); the threshold is set to be higher than the melting point of titanium (1941 K) and to ensure reaction self-propagation (above 2000 K [12]), plus an arbitrary ~500 K margin

- Readily available powder with similar particle size to the Al powder in use (~30 μm)
- Stable in laboratory conditions (air, room temperature)

Thermodynamic data of the thermites was taken from the work of Fischer and Grubelich [12]. Information regarding health hazards and toxicity was recovered from the Safty Data Sheets (SDS) of the investigated substances from major powder manufacturers. The top ranking oxides in terms of matrix volume fraction are reported in Table 1. Some of the best options according to that metric were discarded due to their associated health hazards. They might be worth considering if that constraint were to be relaxed. Out of the remaining options, tungsten trioxide (WO_3) was selected as it represents the best candidate according to the aforementioned criteria.

The characteristics of the powders employed in the experimental campaign are reported in Table 2. The Table also reports the specifics of the Fe_3O_4 powder used in previous work [24], as direct comparison between the different oxides' particle size and their influence on sintering is addressed. The powders have been carefully mixed by hand, as it was observed that resonant acoustic mixing provoked separation of the two species due to the great difference in their specific gravity. Different Al/WO_3 thermite compositions, at 10% oxide weight increments, were tested, as reported in Table 3. The additive (oxide) volumetric content was kept within what is thought to be the threshold for successful sintering of the composite, according to the literature [21].

Oxide	**Al Volume Fraction**	**Health hazard**	**Adiabatic Temperature [K]**	**Gas prod. [%]**	**Notes**
B_2O_3	0.414	✗	2327	0.00	
CoO	0.494	✗	3201	2.54	
Co_3O_4	0.524	✗	3201	12.94	
Cr_2O_3	0.407	✓	2327	0.00	
Fe_2O_3	0.396	✓	3135	7.84	Listed as -325 mesh, actual size is much finer (D05 = 0.45 μm).
MnO_2	0.435	✓	2912	44.70	
MoO_3	0.394	✗	3253	24.73	
Ta_2O_5	0.382	✓	2452	0.00	
TiO_2	0.414	✓	1752	0.00	
WO_2	0.400	✓	3253	6.75	Easily oxidizes to WO_3.
WO_3	0.382	✓	3253	14.63	Readily available, micrometric.

Table 1: Highest ranking oxides in alphabetical order and their relevant properties. Ranking is based on the volume fraction of Al over the total volume of the stoichiometric thermite with the reported oxide (higher is better). The entries evidenced in red do not satisfy the corresponding selection criterion.

Powders	**Manufacturer**	**Purity**	**Characteristics**	**Theoretical Density**
Al	AMG Alpoco	≥ 99%	Spherical, 30 μm (D0.5 = 36.30 μm*)	2.71 g/cm^3
WO_3	Sigma Aldrich	≥ 99%	≤ 25 μm (D0.5 = 44.50 μm*)	7.16 g/cm^3
Fe_3O_4 **	Thermo Scientific	≥ 97%	-325 Mesh (D0.5 = 1.5 μm*)	5.17 g/cm^3

Table 2: Characteristics of the starting ingredients. *: property measured during this work, using a Malvern Mastersizer 2000. **: For reference, employed in previous work by the authors [24].

3.2 Pellet Production

The powders were shaped into pellets, denominated as *greens*, using a hydraulic press. Two different sizes of circular dies were used, with an internal diameter of 8 mm and 3 mm, to produce samples for the mechanical characterization and ignition tests, respectively. The dies were single action and made of hardened D2 tool steel. All samples were

Composition	Ox. mass fraction [%]	Ox. volume fraction [%]	Theoretical Density [g/cm^3]
Al	/	/	2.71
Al + WO_3	10	4.01	2.91
	20	8.60	3.16
	30	13.87	3.46
	40	20.03	3.82
	50	27.28	4.26
	60	36.02	4.84

Table 3: Powder compositions. Oxide volume fraction is computed assuming perfect packing.

produced using an internal die pressure of 250 MPa. Different compositions at increasing oxide mass fraction (from 0% to 60% with 10% increments) were tested. The 8 mm pellets were produced using a nominal total mass of 1 g of powder, while the 3 mm ones contained 50 mg of thermite. A lubricant (WD-40) was applied on the dies in order to avoid galling due to the highly reactive Al, as prescribed by the die manufacturer.

The green pellets were sintered in a HTSolutions HT-S1 furnace on a sample holder made of alumina. The sintering conditions were the following:

- Temperature: ~10°C/min ramp up to 600°C. Temperature was kept constant for 120 minutes. At the end of the heating cycle, the heater was turned off and cooling was allowed to happen naturally with unrestricted rate.

- Atmosphere: high-vacuum ($< 10^{-6}$ bar) was performed inside the furnace, then the heating cycle started. After cool-down, mild vacuum was kept while waiting for an operator to unload the furnace.

Each pellet was weighted and measured with a micrometer (height and diameter) before and after sintering.

3.3 Microscope observation

Samples produced by pressing and sintering were observed through a SEM with Energy Dispersive X-ray (EDX) capabilities (Zeiss EVO 50XVP w/ Oxford Inca Energy 200). The specimens were encased inside a cold mounting resin (QPREP QPOX 92 from QATM/Verder Scientific) and subject to several cycles of vacuum and atmospheric pressure. The procedure allowed to de-gas the porosity of the pellets and allow the resin to fully penetrate and stabilize them. The resin blocks were then sanded and lapped with the aid of a polishing compound.

3.4 Mechanical characterization

Compression tests were conducted using a universal testing machine (MTS model 810) at a constant displacement rate of 1 mm/min. For each composition, three sintered and three green pellets were evaluated. The yield strength and Young's modulus were determined from the stress–strain curves in accordance with ASTM E9-19, which specifies procedures for compression testing of metallic materials at room temperature [27].

Displacement measurements were obtained with an extensometer (MTS model 634.31F-24) mounted on a custom-designed jig replicating the motion of the compressing faces. This setup was necessary because the small dimensions of the specimens did not allow direct attachment of the extensometer (see Figure 1). In addition, three reference pellets were machined from a solid billet of aeronautical-grade aluminum alloy, with dimensions identical to those of the sintered samples.

The experimental procedure generally followed ASTM E9-19, but with two intentional deviations. First, the pellets were fabricated with an aspect ratio of 1, rather than the standard's recommended ratio above 2. Specimens with higher aspect ratio were produced and later discarded due to visible compaction gradient along the pressing direction, likely caused by friction between the powder and the die surface. Second, the standard calls for the use of hardened, surface-ground steel plates and lubricants to minimize friction and maintain uniaxial stress conditions. Since such equipment was unavailable, a standard steel plate was used instead, without lubrication or surface treatment. This led to a pronounced barreling of the specimens. Consequently, the reported results are interpreted as relative comparisons between the thermite and the machined alloy pellets rather than as absolute material properties. The computational procedure followed exactly the prescriptions of ASTM E9-19.

Figure 1: Compression test jig in use.

3.5 Ignition temperature determination

The ignition temperature of both loose powder and sintered pellets was measured. Each sample was positioned on top of a resistive FeCrAl strip, which was heated through a DC power supply by Joule effect until either thermite ignition or failure of the strip (around 1300-1400 °C). Pellets were kept in position through a small wire clip. The power supply was manually regulated to obtain an approximately linear heating of the strip in the range of 40-50 K/s. Such values are representative of the heating rates that can be expected for a medium-sized spacecraft component during re-entry [28]. The surface of the strips was coated using a thermographic paint of known emissivity (LabIR HERP-HT). The temperature of the strips was monitored with a pyrometer (IMPAC IGAR 6) focused near the contact point between the strip and the sample. The tests were conducted in air at room temperature. High speed videos (240 FPS) of the ignitions were recorded. Four sintered pellets were produced and tested for each composition.

4. Results and discussion

4.1 Microscope observation

Figure 2 shows a magnified section view of sintered thermite pellets made of Al/Fe_3O_4 and Al/WO_3. The difference between the dispersion of the two oxides in the pellets is immediately apparent. The fine iron oxide powder spreads in the interstices between the coarser aluminum particles, obstructing the interfaces, and hindering diffusion bonding. Moreover, a strong segregation phenomenon is visible (Figure 2a). On the other hand, the micrometric tungsten trioxide particles populate the aluminum matrix evenly, without interfering in the aluminum-aluminum interfaces (Figure 2b). The homogeneous dispersion of the oxide inside the matrix is very likely responsible for better mechanical properties of the sintered piece.

It has to be noted that the Al/WO_3 composition presents a greater void fraction with respect to Al/Fe_3O_4, as the former behaves similarly to a monomodal powder, which is known to achieve lower density when compared to a bimodal one [29, 30].

4.2 Dimensional analysis

The dimensional changes of the pellets after the sintering phase are reported in Figure 3, together with the densities of the sintered pieces computed as a fraction of the TMD. Six 8 mm pellets for each composition were evaluated.

A slight swelling in both dimensions can be noticed. Densification is usually expected after sintering, as shrinkage a consequence of diffusion bonding between aluminum particles [31, 32]. The observed expansion is believed to be caused by a crystalline phase change of tungsten trioxide. In fact, when heated from room temperature to 550°C, the crystal lattice of WO_3 transitions from the δ to the β phase, increasing its volume from 422.5 $Å^3$ to 432.7 $Å^3$ (going throuh the intermediate γ phase at 250°C, 428.3 $Å^3$) [33].

The effect is amplified at higher WO_3 fractions, and this is also reflected in the overall TMD fraction. Despite the measured expansion, the sintered pellets achieve a high density ($\geq$ 75% TMD).

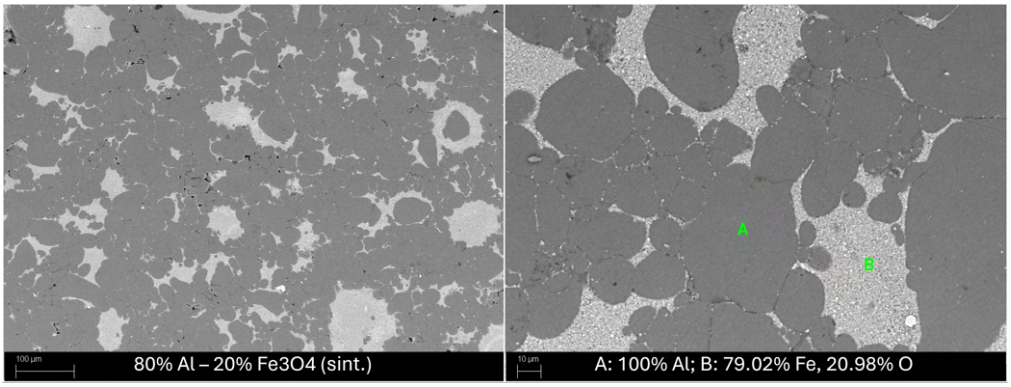

(a) Al/Fe_3O_4 thermite.

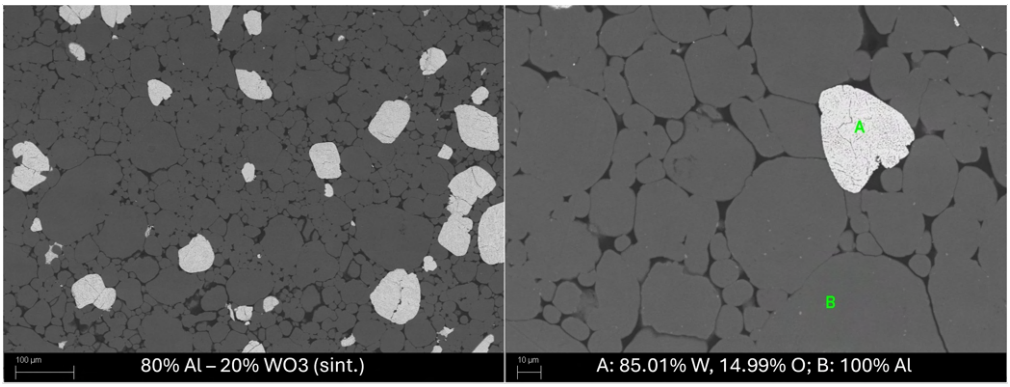

(b) Al/WO_3 thermite.

Figure 2: SEM-EDX images (back-scattered electrons detection) of sintered Al/Fe_3O_4 and Al/WO_3 thermite with 20% oxide mass fraction.

4.3 Uniaxial compression testing

During uniaxial compression, all the sintered Al/WO_3 samples showed significantly improved plasticity with respect to their green counterparts. The stress-strain curves are reported in Figure 4. All the cylinders showed a significant barreling effect, due to their low aspect ratio. The specimens with oxide fraction up to 40% started showing thin surface cracks at 7-10% axial deformation. The samples with 50 and 60% oxide loading fractured earlier and lost fragments from the lateral surface. Despite fracturing, all the sintered samples continued to oppose to the displacement of the pressing jig, contrarily to the greens. This is evidenced by the fact that the stress curves of the sintered pieces does not decrease after yielding of the material, like it happens with the greens.

The computed values of the yield stress and the Young modulus of the sintered pellets are reported in Figure 5. All composite formulations have significantly lower elasticity modulus than pure Al, and the material becomes less rigid as the oxide fraction is increased. This was expected, as the additive is thought to worsen the sintering effectiveness. Accordingly, the yield stress rises as the oxide content is increased (and rigidity is reduced). However, it appears that the yield stress plateaus at 40% WO_3 fraction and decreases at higher concentrations. This is in accordance with the visual observations of the tests, where earlier cracking and fragmentation of those samples was recorded.

The presented results show that proper selection of the oxide particle size is crucial for thermite sintering. Sintered pellets containing the finer Fe_3O_4 tested previously were extremely fragile, even at very low oxide content, and performed only marginally better than greens [24].

4.4 Ignition testing in air

Thermite pellets containing 20%, 30%, and 40% of WO_3 were sintered and ignited. The measured ignition temperatures are illustrated in Figure 6. All the pellets ignited successfully near 1200°C, irrespectively of the thermite O/F ratio. The corresponding loose powders ignited at similar, but slightly lower, temperatures. However, loose powder

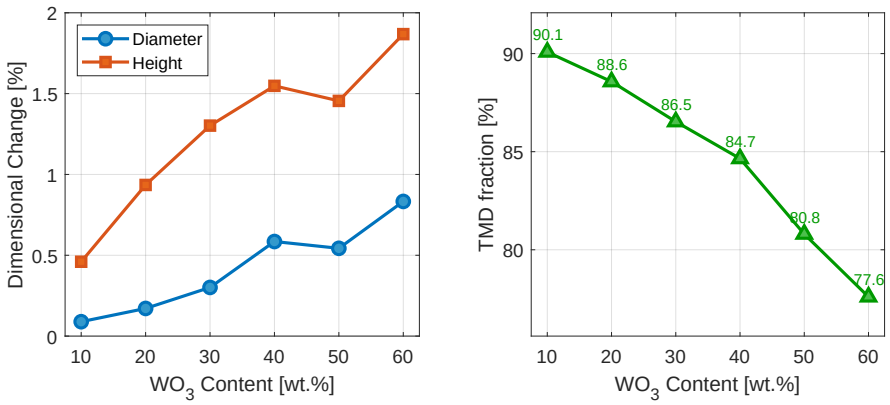

Figure 3: Dimensional change of the pellets after sintering. Positive values indicate an increase in the indicated dimension. On the right, sintered pellet density as a fraction of the TMD.

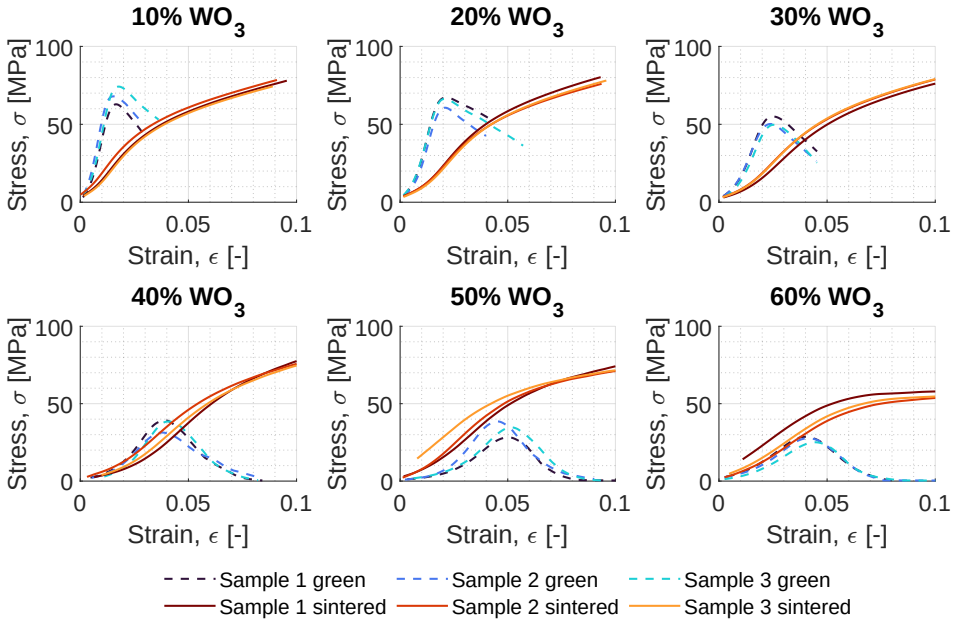

Figure 4: Experimental stress-strain curves of sintered and green Al/WO_3 pellets.

ignition was unreliable when decreasing the oxide fraction. The composition with 20% oxide content could not be ignited, and the hot wire always broke first.

This effects can be attributed to the compaction, leading to the deformation of the starting spherical particles, the increase of thermal conductivity, and the creation of intimate fuel-oxidizer interfaces thanks to the Al sintering. It is acknowledged that micrometric thermites exhibit faster propagation speeds at higher density (particularly, when above 65% of TMD) [34]. Reactive sintering is recognized as one of the main reaction mechanisms in nano- and micron-sized Al-based thermites, contributing to faster combustion waves [35]. It is hypothesized that introducing sintering in the manufacturing of thermite pellets yields reduced diffusion barriers. As a consequence, sintered samples ignite readily even in extremely fuel rich conditions. It is thought that the excess fuel reacts with ambient oxygen only after being triggered by the thermite reaction, since micrometric Al of 30 μm size is reportedly difficult to ignite in air [36]. Therefore, the enhanced fuel-oxidizer interface provided by sintering allows the combustion to start and propagate easily, while the loose powder does not ignite.

Two different combustion behaviors were identified during the ignition tests of sintered pellets, which are reported in Figure 7 as still frame sequences. In the first type of reaction (7a), pellets heated up starting from the contact surface with the strip until ignition. The ignition generated a moderate flash and a modest amount of sparks, and the reaction proceeded as a small, slow burning flame on the surface of the pellets. This kind of reaction mechanism did not cause the destruction of the pellet nor of the heating strip, and it was denominated "non-demising". The second type of combustion (7b) evolved much more violently, generating a substantially bigger flame which quickly propagated and

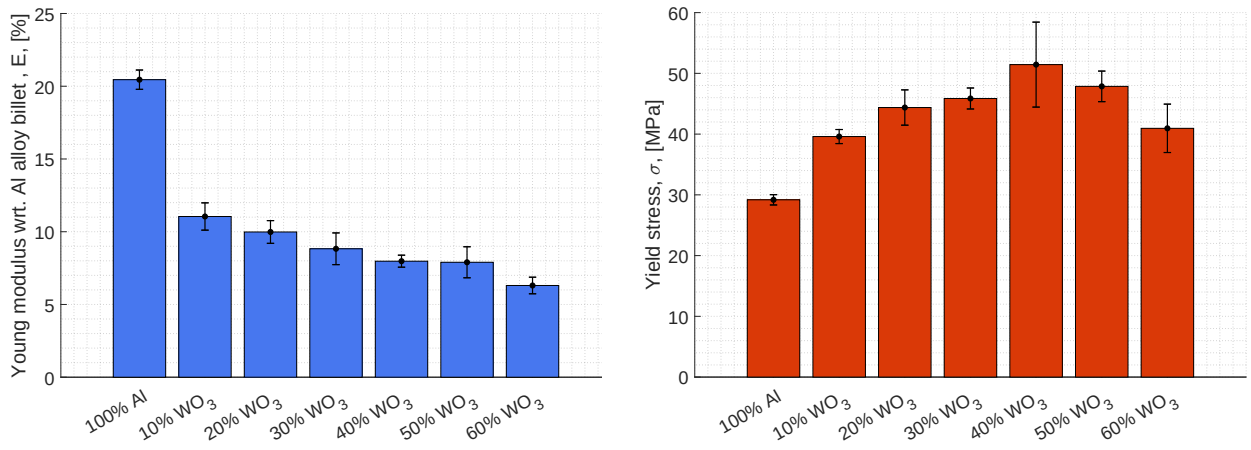

(a) Normalized Young's modulus.

(b) Yield stress.

Figure 5: Mechanical properties of sintered Al/WO_3 thermite pellets: (a) normalized Young's modulus and (b) yield stress.

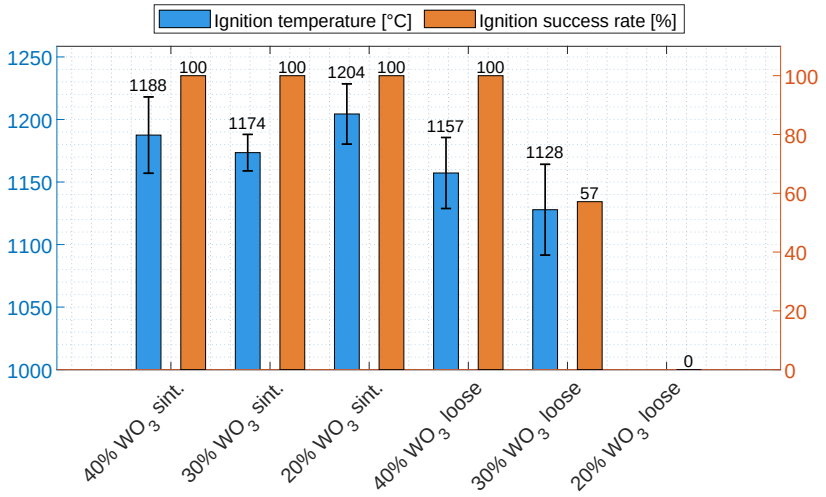

Figure 6: Ignition temperatures of the sintered thermite pellets and corresponding loose thermite powder in air.

melted the resistive strip and the pellet itself. This type of behavior was denominated "demising".

All the pellets with 40% oxide content showed demising combustion, while the others exhibited both behaviors. However, no statistically valid conclusions can be derived due to the small sample size.

It was hypothesized that, for both reaction types, the ignition is sparked by the thermitic redox reaction, as evidenced by the fact that the ignition temperature is roughly the same across all the samples. Moreover, micrometric Al does not ignite easily in the same conditions, as already mentioned. The reaction then evolves into either the demising or non-demising case depending on the oxidizer-to-fuel ratio, the homogeneity in the oxide distribution inside the matrix, or both. If the O/F is sufficiently high or if the oxide is evenly dispersed across the volume of the pellet, the thermitic reaction propagates, releases enthalpy, and the excess fuel burns in air, evolving in the demising scenario. If the O/F is too low or if the oxide distribution is uneven, the thermitic reaction does not propagate. Some excess Al is burnt, but mostly it is oxidized to alumina due to the high temperature and oxidizing atmosphere. In this case, the reaction is non-demising. This hypothesis is corroborated by observing the pellets after non-demising combustion, which feature a white shell resembling alumina (Figure 8).

Further investigation is needed to confirm this hypothesis, involving diagnostics such as tomography to asses the oxide distribution, differential thermal analysis in oxidizing and inert atmosphere, and X-ray diffraction analysis of the burned specimens.

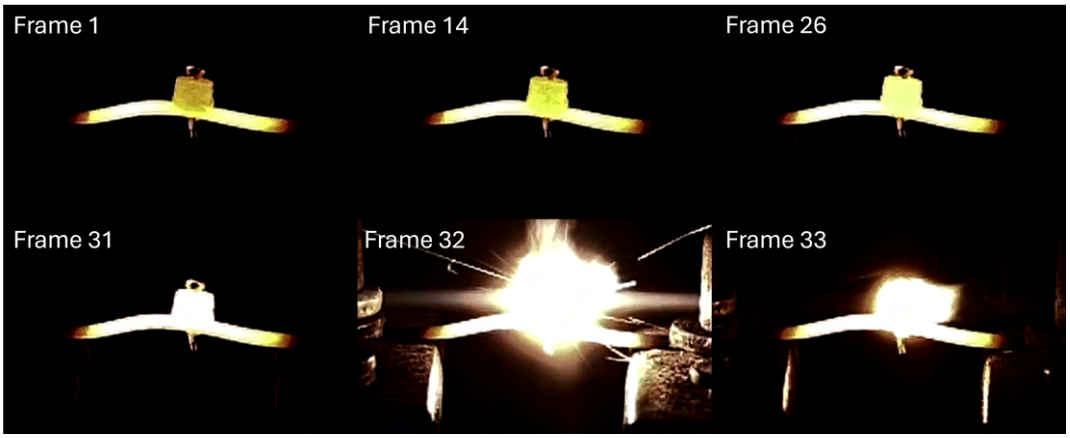

(a) "Non-demising" combustion.

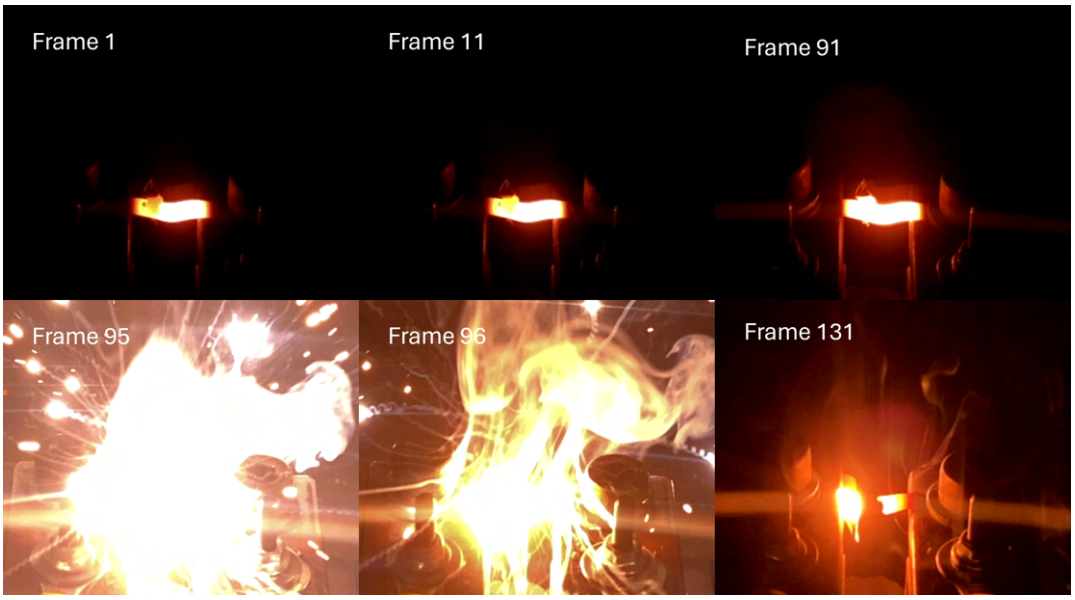

(b) "Demising" combustion.

Figure 7: Sintered thermite pellet ignition sequences.

Figure 8: Sintered thermite pellet after non-demising combustion.

5. Conclusions

Aluminum/tungsten trioxide thermite was selected as a suitable candidate for the production of shape-retaining sintered composite pellets, according to criteria such as matrix-to-additive ratio, particle size distribution, and minimal health hazard. The specimens, produced by single action pressing and sintering in high vacuum, were characterized for their mechanical properties and ignition temperature. The O/F ratio of the pellets was varied to explore the effect of this variable on their mechanical characteristics and reactivity.

Microscope images revealed that matching the particle size between the matrix and the additive was essential to avoid interference in diffusion bonding. It was observed that the pellets expand after sintering, possibly due to crystalline phase change of WO_3 at high temperature. Relatively high compaction was reached, ranging from 75% to 90% depending on the oxide content. Sintered pellets exhibited greatly improved mechanical characteristics with respect to greens at all WO_3 concentrations, although the samples fractured more easily and performance decreased over 40% oxide fraction.

The ignition temperature in air of sintered pellets was measured to be around 1200°C, with little variation between different O/F. Slightly lower temperature was registered for the loose powders. The pellets achieved 100% ignition success, whereas the most fuel rich powders could not be ignited. It is hypothesized that the introduction of sintering in the manufacturing process reduces diffusion barriers and facilitates the ignition and propagation of the thermitic reaction. The high compaction likely concurs to the same result.

Two different combustion behaviors were observed: a more violent one, denominated "demising", which leads to complete destruction of the pellet and the heating strip, and milder one, called "non-demising". Both are thought to be primed by thermite ignition. The evolution towards one or the other behavior is attributed to differences in O/F and oxide distribution within the volume of the pellets. Larger sample size and tailored diagnostics are needed to fully characterize this phenomenon.

6. Acknowledgments

The authors sincerely thank Mr. Alberto Verga and Mr. Paolo Rubini for their support during the experimental activity.

Funded by the European Union through the European Innovation Council (EIC) within the THREAD project (Grant agreement ID: 101186901). Views and opinions expressed are however those of the authors only and do not necessarily reflect those of the European Union or the European Innovation Council (EIC). Neither the European Union nor the granting authority can be held responsible for them.

Bibliography

[1] Anon. *ESA's Annual Space Environment Report*. Tech. rep. GEN-DB-LOG-00288-OPS-SD. Darmstadt, Germany: European Space Agency, 2025.

[2] Anon. *IADC Report on the Status of the Space Debris Environment*. Tech. rep. IADC-23-01, Issue 2, Rev. 0. Inter-Agency Space Debris Coordination Committee, 2024.

[3] D. J. Kessler and B. G. Cour-Palais. "Collision Frequency of Artificial Satellites: The Creation of a Debris Belt". In: *Journal of Geophysical Research* 83(A6) (1978), pp. 2637–2646.

[4] Anon. *Space Innovation; Mitigation of Orbital Debris in the New Space Age*. Tech. rep. FCC-CIRC2209-01. Federal Communications Commission, 2022.

[5] V. V. A. A. *ESA Space Debris Mitigation Requirements*. Tech. rep. ESSB-ST-U-007, Issue 1, Rev. 0. European Space Agency, 2023.

[6] S. Perrault, T. Soares, and L. Innocenti. "Re-entry strategies to comply with Space Debris Mitigation guidelines". In: *First International Orbital Debris Conference*. Sugar Land, Texas, USA, 2019.

[7] B. M. Cattani et al. " An Overview of Design for Demise Technologies". In: *8th European Conference on Space Debris*. Darmstadt, Germany, 2021.

[8] A. Finazzi et al. “Thermite-for-Demise (T4D): Experiments and numerical modelling on ball-bearing unit mock-ups containing thermite in an arc-heated wind tunnel”. In: *Acta Astronautica* 223 (2024), pp. 550–576. DOI: https://doi.org/10.1016/j.actaastro.2024.06.013.

[9] M. J. M. M. Steenbergen and R. W. van Bezooijen. “Wheel-rail Interface Handbook”. In: Cambridge, UK: Woodhead Publishing in Mechanical Engineering, 2009. Chap. 12 - Rail welds.

[10] S. Turner. *Thermite cutting device*. Patent GB 2312864 A. 1997.

[11] J. C. Carter Jr. *Portable metal cutting pyrotechnic torch*. Patent US 2003/0145752 A1. 2003.

[12] S. H. Fischer and M. C. Grubelich. “Theoretical energy release of thermites, intermetallics, and combustible metals”. In: *24th International Pyrotechnics Seminar*. Monterey, California, USA, 1998.

[13] D. Dilhan and P. Omaly. *Élement de véhicule spatial a capacité d’autodestruction ameliorée et procedure de fabrication d’un tel elément*. Patent FR 2975080B1. 2011.

[14] R. Seiler and G. Smet. *Exothermic reaction aided spacecraft demise during reentry*. Patent EU 3604143A1. 2018.

[15] A. Finazzi et al. “Thermite-for-Demise (T4D): experiments and numerical modelling on solar array drive mechanism mock-ups containing thermite in an arc-heated wind tunnel”. In: *CEAS Space Journal* (2025). DOI: https://doi.org/10.1007/s12567-025-00598-8.

[16] K. A. Monogarov et al. “Pyrotechnic approach to space debris destruction: From thermal modeling to hypersonic wind tunnel tests”. In: *Acta Astronautica* 172 (2020), pp. 47–55. ISSN: 0094-5765. DOI: https://doi.org/10.1016/j.actaastro.2020.03.028.

[17] T. Schleutker et al. *ERASD – Exothermic Reaction Aided Spacecraft Demise – Proof of Concept Testing*. Tech. rep. DLR, Supersonic and Hypersonic Technologies Department, 2019.

[18] D. L. Hastings and E. L. Dreizin. “Reactive Structural Materials: Preparation and Characterization”. In: *Advanced Engineering Materials* 20 (2018), p. 1700631.

[19] K. E. Neely, A. M. Strauss, and K. C. Galloway. “Additively manufactured reactive material architectures for exothermic brazing”. In: *Additive Manufacturing Letters* 1 (2021), p. 100005. ISSN: 2772-3690. DOI: https://doi.org/10.1016/j.addlet.2021.100005.

[20] C. Gosselin et al. “Large-scale 3D printing of ultra-high performance concrete – a new processing route for architects and builders”. In: *Materials and Design* 100 (2016), pp. 102–109. ISSN: 0264-1275. DOI: https://doi.org/10.1016/j.matdes.2016.03.097.

[21] R. M. German. “Chapter Eleven - Mixed Powders and Composites”. In: *Sintering: from Empirical Observations to Scientific Principles*. Boston: Butterworth-Heinemann, 2014, pp. 355–385. ISBN: 978-0-12-401682-8. DOI: https://doi.org/10.1016/B978-0-12-401682-8.00011-2.

[22] A. Agostinelli. “Reactivity characterization of nanometric and activated Al-based thermites”. MA thesis. Politecnico di Milano, 2020.

[23] N. Llorca-Isern and C. Artieda-Guzmán. “Metal-based composite powders”. In: *Advances in Powder Metallurgy*. Sawston: Woodhead Publishing, 2013, pp. 241–272. ISBN: 978-0-85709-420-9. DOI: https://doi.org/10.1533/9780857098900.2.241.

[24] A. Finazzi et al. “Thermite-for-Demise (T4D): Thermite charge shaping advancements”. In: *11th European Conference for Aeronautics and Space Sciences (EUCASS)*. Rome, Italy, 2025. DOI: 10.13009/EUCASS2025-716.

[25] Anon. *Yield Strength of Aluminum Alloys*. Online. https://www.sunrise-metal.com/yield-strength-of-aluminum-alloys/ [Accessed: 12/06/2025].

[26] H. Breulet and T. Sinaba. “Explosivity and Flammability of Nanopowders: New Challenges”. In: *Chemical Engineering Transactions* 77 (Sept. 2019), pp. 223–228. DOI: 10.3303/CET1977038.

[27] Anon. *Standard Test Methods of Compression Testing of Metallic Materials at Room Temperature*. ASTM Standard E9-19. West Conshohocken, PA, 2025. DOI: 10.1520/E0009-19.

[28] A. Finazzi et al. “Thermite-for-Demise (T4D): Material selection for exothermic reaction-aided spacecraft demise during re-entry”. In: *2nd International Conference on Flight Vehicles, Aerothermodynamics and Re-entry Missions and Engineering (FAR)*. Heilbronn, Germany, 2022.

[29] L. Chen et al. “Effect of bimodal powder on densification and mechanical properties of 316L stainless steel fabricated by binder jet 3D printing”. In: *Journal of Materials Research and Technology* 27 (2023), pp. 4043–4052. ISSN: 2238-7854. DOI: https://doi.org/10.1016/j.jmrt.2023.10.203.

[30] Y. Bai, G. Wagner, and C. Williams. “Effect of bimodal powder mixture on powder packing density and sintered density in binder jetting of metals”. In: *26th International Solid Freeform Fabrication Symposium*. Austin, TX: University of Texas at Austin, 2015.

[31] V. A. Invenson. *Densification of metal powders during sintering*. Springer Science & Business Media, 2012.

[32] R. German and A. Bose. “Sintering Densification”. In: *Binder and polymer assisted powder processing*. ASM International, 2020, pp. 169–191. ISBN: 978-1-62708-319-5. DOI: https://doi.org/10.31399/asm.tb.bpapp.9781627083195.

[33] T. Vogt, P. M. Woodward, and B. A. Hunter. “The high-temperature phases of WO3”. In: *Journal of Solid State Chemistry* 144.1 (1999), pp. 209–215.

[34] M. L. Pantoya et al. “Effect of Bulk Density on Reaction Propagation in Nanothermites and Micron Thermites”. In: *Journal of Propulsion and Power* 25.2 (Mar. 2009). Number: 2, pp. 465–470. ISSN: 0748-4658, 1533-3876. DOI: 10.2514/1.36436.

[35] K. T. Sullivan et al. “Reactive sintering: An important component in the combustion of nanocomposite thermites”. In: *Combustion and Flame* 159.1 (Jan. 2012), pp. 2–15. ISSN: 00102180. DOI: 10.1016/j.combustflame.2011.07.015.

[36] J.-w. Qian et al. “Ignition and Combustion Characteristics of Micro-Aluminum and Nano-Aluminum Mixture”. In: *Propellants, Explosives, Pyrotechnics* 50.7 (2025), e12077. DOI: https://doi.org/10.1002/prep.12077.